https://doi.org/10.5194/egusphere-2026-1813
Preprint. Discussion started: 11 May 2026

Isotope-based investigation of methane sources in Hamburg, Germany

Jacoline van Es[1], Juan Bettinelli[2], Jia Chen[2], Carina van der Veen[1], Stephan Henne[3], and Thomas Röckmann[1]

[1]Institute for Marine and Atmospheric Research Utrecht (IMAU), Utrecht University, Utrecht, the Netherlands
[2]Technische Universität München, Arcisstraße 21, 80333 München
[3]Swiss Federal Laboratories for Materials Science and Technology (Empa), Dübendorf, Switzerland

Correspondence: Jacoline van Es (j.d.vanes@uu.nl) and Jia Chen (jia.chen@tum.de)

Abstract.

Methane (CH_4) is the second most important anthropogenic greenhouse gas and reducing CH_4 emissions can lead to climate benefits on the timescale of a decade. Knowledge of the most important sources in different regions is important for designing and implementing successful mitigation strategies. We present a detailed investigation into the source mix of CH_4 emissions in Hamburg, Germany, using measurements of the CH_4 mole fraction and isotopic composition by combining data from multiple observational campaigns and an atmospheric transport model. Measurements of CH_4 isotopic composition were performed for eight months using isotope-ratio mass spectrometry (IRMS) at the Geomatikum building in the city centre, 82 m above ground level. The isotopic composition clearly demonstrates that the observed CH_4 enhancements originated mainly from microbial sources. Supporting meteorological and hydrological data provide context for explaining the temporal CH_4 variability. The highest observed CH_4 enhancements are sharp peaks from microbial sources that occur only during low tides and when air is advected from the south, where the Elbe River and the Hamburg harbour are located. Measurements with a mobile analyser along the river confirm that large emissions occur from the banks of the Elbe River during low tides. Our integrated approach demonstrates the benefit of combining detailed measurements (isotopes and mobile) and high-resolution modelling for accurately attributing greenhouse gas sources in complex environments.

1 Introduction

Methane (CH_4) is a potent greenhouse gas with a global warming potential of about 84 over a 20-year timescale and an atmospheric lifetime of about 9 years (Saunois et al., 2020). The increase in CH_4 emissions since pre-industrial times has contributed about 0.6°C to the observed global warming (Calvin et al., 2023). The ongoing increase in atmospheric CH_4 undermines efforts to mitigate climate change. The goals of the Paris Climate Agreement (United Nations, 2016) can only be reached if we reduce the CH_4 emissions and lower atmospheric CH_4 levels (Rogelj and Lamboll, 2024). To effectively mitigate CH_4, it is essential to understand its sources.

A widely used method to distinguish emissions from different source categories is measuring the CH_4 isotopic composition. Such measurements provide additional insight as different CH_4 production processes emit CH_4 with different isotopic

https://doi.org/10.5194/egusphere-2026-1813
Preprint. Discussion started: 11 May 2026

composition (Whiticar, 2020). Generally, CH_4 produced by microbial processes contains slightly less of the heavy carbon and hydrogen isotopes than CH_4 formed thermogenically and even less than CH_4 released during incomplete combustion from pyrogenic processes. Traditionally, CH_4 isotope measurements have been carried out on atmospheric air samples in the laboratory, but since a few years, instruments measuring isotopic composition in situ have become available (Röckmann et al. (2016), Menoud et al. (2021), van Es et al. (2025), Eyer et al. (2016)).

An important application of continuous isotopic CH_4 measurements is the evaluation of emission inventories. Atmospheric transport models can use these emission inventories to explicitly calculate the relative contributions of different source categories to observed CH_4 enhancements. Since each source emits CH_4 with a characteristic isotopic signature, it is possible to derive a simulated time series of the isotopic composition of atmospheric CH_4 from the source contributions. By comparing these simulations with observed isotopic data, we cannot only assess whether total emissions in a model are over- or underestimated, but also identify which source categories are responsible for any discrepancies.

In this study, we focus on the city of Hamburg, Germany. Cities are hotspots of greenhouse gas emissions like CH_4, but it is difficult to determine the relative contribution of different processes because many sources emit in proximity (Hopkins et al., 2016). Therefore, new approaches are being developed to better characterise the dynamics of CH_4 and other greenhouse gas emissions in cities, including isotopic source attribution (van Es et al. (2025), Menoud et al. (2021), Dietrich et al. (2023)). In Hamburg, previous research identified CH_4 emissions associated with natural gas leaks and biogenic sources from measurements at the street level with mobile high-precision in-situ sensors (Maazallahi et al., 2020). In addition, important contributions from the Elbe River and associated wetland emissions were discovered and quantified using total column measurements, isotopic measurements, and an inverse modelling approach (Forstmaier et al., 2023). The observed enhancements could be explained by an atmospheric inverse modelling system when the prior estimates on emissions from one part of the Elbe River (Matoušů et al., 2017) were substantially increased.

We present a comprehensive investigation of atmospheric CH_4 and its key sources in Hamburg through long-term monitoring of the isotopic composition, coordinated field campaigns and integrated data analyses. By combining different observational measurement strategies, meteorological and hydrological data and atmospheric transport simulations, we characterise the main CH_4 emission sources and interpret unexpected CH_4 enhancements to improve our understanding of urban CH_4 emissions.

2 Methods

CH_4 emissions in Hamburg have been targeted by several scientific investigations in recent years. Table 1 provides an overview of the different campaigns and observational and modelling systems that were either performed for this study or referred to and used in the data interpretation.

2.1 Continuous measurement location

Hamburg is Germany's second-largest city with approximately 1.9 million inhabitants. Its position along the Elbe River and the presence of the Alster and Bille tributaries not only shape the city's landscape but have historically established Hamburg

https://doi.org/10.5194/egusphere-2026-1813
Preprint. Discussion started: 11 May 2026

Campaign/dataset	Variables	Location	Purpose	Period
Continuous isotope campaign	χCH_4, ^{13}C, ^{2}H	Geomatikum	Primary dataset	08-2021 to 04-2022,
FLEXPART simulations	χCH_4, ^{13}C, ^{2}H	Geomatikum	Comparison with Primary dataset	08-2021 to 04-2022,
Short-term stationary	χCH_4	In-situ at locations 1-10 (Fig. 1)	Identification of river emissions	04-2024 to 05-2025
Bag samples	χCH_4, ^{13}C, ^{2}H	In-situ at locations 1-10 (Fig. 1)	Isotopic composition of river emissions	04-2024 to 05-2025
Picarro	χCH_4	Geomatikum	Comparison with previous continuous CH_4 measurements	04-2024 to 05-2025
Water level	Water level	St. Pauli	Relation to CH_4 emissions	During both Geomatikum CH_4 measurements
Meteorological	Wind direction and wind speed	Geomatikum	Relation to CH_4 emissions	During both Geomatikum CH_4 measurements
Meteorological	Boundary Layer height	Geomatikum	Relation to CH_4 emissions	08-2021 to 09-2021
FTIR from Forstmaier et al. (2023)	Total column mole fraction CO_2, CH_4 and CO	Four locations throughout the city	Simulations for Forstmaier et al. (2023)	27-07-2021 to 09-09-2021
Wind Lidar	χCH_4	In-situ at locations 1-10 (Fig. 1)	origin of the wind	04-2024 to 05-2025

Table 1. Table with the summary of all campaigns and datasets used in this study. χCH_4 refers to CH_4 mole fraction.

as a centre of commerce and maritime activity. Beyond the city limits lies extensive farmland. The region is not known for extensive mining, however, resources like peat and clay have been historically significant and could potentially emit CH_4. The wider region surrounding Hamburg also features some coastal wetland areas to the northwest. This combination of diverse potential sources makes measuring CH_4 isotopes a useful tool to identify emissions form the different sources.

The continuous isotope measurement system developed and operated by Utrecht University (Röckmann et al., 2016) was placed inside a laboratory on the top floor of the Geomatikum, the tallest building of the University of Hamburg. At ground level, the Geomatikum is elevated approximately 19 m above the river level in the city centre of Hamburg at 53° 34’ 5.13"N, 9° 58’ 27.4"E. With 83 m, the building reaches above the urban canopy layer. No similarly tall buildings are present in the immediate vicinity, reducing the influence of local vertical obstructions. The area around the building is predominantly residential. South of the Geomatikum, on the opposite side of the Elbe River, lies the Port of Hamburg. Located approximately 115 km

https://doi.org/10.5194/egusphere-2026-1813
Preprint. Discussion started: 11 May 2026

inland from the North Sea along the course of the Elbe, the port is still subject to tidal influences. As a result, water levels fluctuate significantly and the river banks are exposed during low tide. The Port of Hamburg is characterised by extensive industrial activity. This includes a variety of facilities such as logistics hubs, oil and gas refineries, and civil infrastructure. To the east of the Geomatikum are the Alster Lake and several artificial channels. Figure 1 displays a high-resolution map of the continuous
7 measurement location and the surroundings in the Web Mercator coordinate reference system (EPSG:3857) (Openstreetmap).

2.2 Measurement approaches

2.2.1 CH_4 isotope measurements

From 01-08-2021 to 01-04-2022, we measured ^{2}H, ^{13}C, and the mole fraction (χCH_4) of atmospheric CH_4 using a custom-built CH_4 extraction and purification system, coupled to an isotope ratio mass spectrometer (IRMS). Air was provided via a
75 1/4" o.d. Dekabon/Synflex line from an inlet mounted at the railing of the outermost edge of the southeast balcony on the 18^{th} (70m) floor of the Geomatikum. The fully automated system sampled 40 or 50 mL of air from the inlet line every 20 minutes, for ^{2}H and ^{13}C respectively. Via a series of cryogenic traps and gas chromatography, the CH_4 was purified from the ambient air before being converted either to hydrogen (H_2) in a pyrolysis oven or to CO_2 in a combustion oven, for ^{2}H or ^{13}C measurements, respectively. These analyte gases were then injected through the ConFlo IV interface into a ThermoFisher
8 Scientific Delta V isotope ratio mass spectrometer (IRMS) for isotope analysis.

The hydrogen and carbon isotopic composition was quantified relative to a working gas with [^{13}C= -48.30‰, ^{2}H = -92.07‰, χCH_4 = 2032 ppb], which was regularly measured after 5 air samples to correct for instrument drift. In addition, we daily measured a target gas [^{13}C= -50.27‰, ^{2}H = -130.60‰, χCH_4 = 2487.0 ppb] after measuring six aliquots of working gas to monitor the instrument stability. CH_4 mole fractions were obtained from the peak area recorded in the IRMS chromatogram.
85 The system achieved reproducibility of better than 10 ppb for CH_4 mole fraction, ± 0.07‰ for ^{3}C and ± 2.3‰ for ^{2}H. More details about the system, the isotope calibration and the data analysis procedures are available in Röckmann et al. (2016) and Menoud et al. (2021).

2.2.2 Measurements near the river

Two years after the initial campaign, from 17-04-2024 to 02-05-2024, we conducted a targeted two-week campaign in Hamburg
9 with mobile equipment to further investigate CH_4 emissions from the Elbe River. Mobile and short-term-stationary measurements were carried out using a MIRA Ultra mobile analyser (Aeris Technologies), measuring both CH_4 and C_2H_6 at 1 Hz, with a sensitivity (1 σ) of 2 ppb/s and 500 ppt/s and a maximum drift in 24 hours of 2 ppb and 3 ppb for CH_4 and C_2H_6, respectively. In addition, the environmental parameters, wind speed and wind direction were measured with a Lufft WS200-UMB5 Smart Weather Sensor during the short-term-stationary measurements.

95 Measurement locations for the short-term stationary measurements were selected daily based on real-time wind direction and wind speed forecasts and tidal cycle predictions for the Elbe River. We aimed to capture CH_4 emissions from exposed riverbed sediments. Therefore, each measurement session was planned to start at high tide and continue through the entire ebb

https://doi.org/10.5194/egusphere-2026-1813
Preprint. Discussion started: 11 May 2026

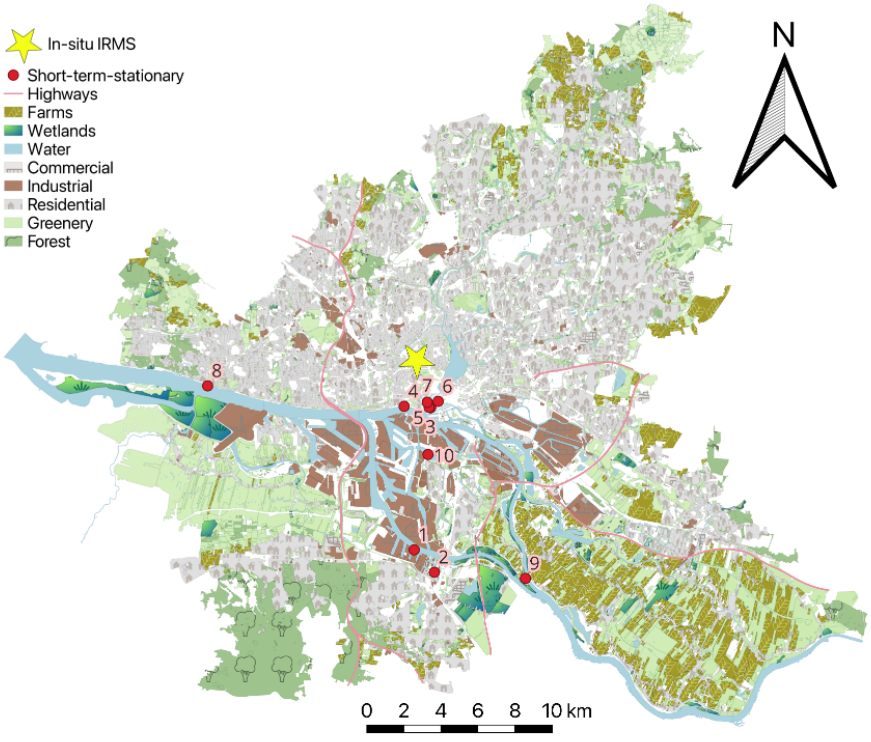

Figure 1. Map of Hamburg (Web Mercator coordinate reference system EPSG:3857) showing the main land use types in the city (indicated in the legend, from Openstreetmap). The yellow star shows the measurement location of the continuous measurements at the Geomatikum building, the red circles show the short-term measurement locations visited with the mobile analyser. Numbers are added to the measurement locations for in-text references.

phase until sediments were fully re-submerged by the incoming water. The measurement locations and the surroundings are shown in Fig. 1.

To confirm that the short-term stationary measured CH_4 actually originated from biogenic processes, as expected for the Elbe River, we collected dry air samples in 2L Supel^{TM} Inert Foil Gas bags for isotopic analysis at the Utrecht University laboratory. We sampled before, after and during low tide to cover CH_4 from both background and elevated samples. In total, 40 air samples were collected at ten different locations. These bags were analysed at Utrecht University using an IRMS system similar to the system used for continuous measurements.

To compare the observations during the short-term stationary campaign in 2024 with the previous continuous isotopic measurements, we installed a Picarro G2301 analyser measuring the CH_4 mole fraction at the Geomatikum. This provides high-frequency baseline measurements of CH_4 mole fraction.

https://doi.org/10.5194/egusphere-2026-1813
Preprint. Discussion started: 11 May 2026

2.3 Additional datasets

Boundary layer height: The atmospheric boundary layer height (BLH) was measured using a Leosphere Windcube 200S
11 Doppler Wind-LiDAR installed at the Hamburg Billbrook weather mast (53 31'9.39"N, 10 6'9.414"E) from 01-08-2021 to 05-09-2021. In addition, and for the remaining period, we analysed the BLH from the ECMWF Reanalysis v5 (ERA5) model (Hersbach et al., 2020), further corrected with wind data from a Leosphere Windcube 200S Doppler wind LiDAR (Wildmann et al. (2020), Vasiljević et al. (2016)).

Wind speed and direction: Wind speed and direction data were obtained from a local wind station located at 1.3 meters dis-
115 tance from the IRMS inlet at an elevation of 80 m and averaged over 10-minute intervals via the Yamartino method (Yamartino, 1984). At this height, surface friction effects are largely minimised; however, the presence of the Geomatikum building itself may introduce localised turbulence that could influence measurements.

Water level: Hourly water levels were obtained from the St. Pauli station (53 32'43.5 "N, 9 57'57.7" E) (Port of Hamburg Marketing).

12 ### 2.4 Data evaluation

2.4.1 Identification of CH_4 enhancements

To enable systematic and reproducible identification of CH_4 enhancements, we applied a peak finding algorithm to the CH_4 mole fraction time series. Peak finding was done with the function find_peaks of the package scgl in Python. Valid peaks had to contain at least five data points. Visual interpretation indicated two categories of peaks, which were identified and
125 characterised using two integration methods. The first category are the sharp peaks, which we define as peaks with a minimum CH_4 enhancement of 400 ppb and a maximum duration of eight hours. The second category, referred to as diurnal peaks, is characterised by a minimum mole fraction elevation of 100 ppb and a maximum duration of 27 hours. These peaks are often related to the diurnal cycle, rising during the night and lowering during the day, but can sometimes persist for more than 24h. For the simulated time series, only the diurnal peak integration is used as the simulated time series did not visually indicate the
13 presence of sharp peaks.

2.4.2 Source signature calculation

We applied the Keeling plot approach (Keeling (1961), Röckmann et al. (2025), Pataki et al. (2003)) to determine the isotopic signature of the source mixing into background air. This mass balance method expresses the total atmospheric CH_4 mole fraction (c) as the sum of background (c_b) and source (c_s) contributions:

135 $$c = c_b + c_s \tag{1}$$

The corresponding mass balance for the minor isotopologue can be approximated as:

$$c = {}_b c_b + {}_s c_s \tag{2}$$

https://doi.org/10.5194/egusphere-2026-1813
Preprint. Discussion started: 11 May 2026

Combining Equations 1 and 2, we obtain the Keeling plot expression:

$$= \frac{c_b}{c} \quad _b \quad _s) + \quad _s \tag{3}$$

This formulation describes a linear relationship between the measured atmospheric isotopic composition and the inverse of the observed atmospheric CH_4 mole fraction ($\frac{}{c}$). The y-axis intercept of a linear fit of vs. $\frac{}{c}$ corresponds to the isotopic signature of the source, $_s$. In our analysis, we applied orthogonal distance regression to the identified CH_4 enhancements, using on the y-axis and $\frac{}{c}$ on the x-axis. The Keeling plot method requires that both the background isotopic composition ($_b$) and the source signature ($_s$) remain constant during the measurement period. While this assumption may not hold over the full timeseries, the background can generally be assumed to be stable for both the duration of a sharp peak and a diurnal peak. This Keeling plot approach was also used for the samples taken near the river. The Keeling plots were considered unreliable when the CH_4 mole fraction elevation was below 20 ppb and excluded from further analysis.

2.5 FLEXPART simulations

The CH_4 was simulated using the Lagrangian particle dispersion model FLEXPART (Stohl et al., 2005) coupled to output from the operational high-resolution analysis (HRES) of the Integrated Forecast System (IFS) operated by the European Centre for Medium Range Weather Forecast (ECMWF). Input fields were available hourly at 0.1°x0.1° resolution for the European domain and at 0.5°x0.5° elsewhere.

Every hour, 20,000 air parcels were released from the location of the Geomatikum building, 80 m above the surface and traced backwards in time for 8 days to compute the sensitivity of each hourly time period to upwind sources. The resulting source sensitivity maps (or footprints) (Seibert and Frank, 2004) were stored with a spatial resolution of 0.02° x 0.01° in a domain of 200 km x 160 km around Hamburg and with a coarser resolution (0.1°x0.1°) elsewhere. Source sensitivities were then multiplied with gridded CH_4 emissions to estimate the mole fraction enhancement above background from different source categories. Emissions were taken either from the TNO-MACC II GHGco inventory for Northern Germany (year 2018, 0.0166° x 0.00833° resolution) or from the TNO-CoCO2 inventory (version 5.0, year 2021, 0.1° x 0.05° resolution) (Kuenen et al., 2022). For the domain covered by the FLEXPART simulations, total anthropogenic emissions in the TNO-MACC inventory are 18.3 Tg CH_4 yr^{-1}. The transport model treats CH_4 emitted from different source categories as distinct tracers, whose contributions sum to the total CH_4.

In addition, river and associated wetland emissions were parametrised as a separate river layer in the emission fields based on Matoušů et al. (2017). The base simulations do not take the effect of tides into account for the river layer, but in a sensitivity calculation, the emissions near low tide were multiplied by a deliberate scaling factor of 100 to simulate strongly increased emissions when the river banks are exposed during low-tide conditions, as detected during the measurements.

When analysing the model results, we assign isotopic source signatures to the emissions from the various source categories. The CH_4 isotopic source signatures were computed separately for several different emitter types and formation mechanisms, as specified within Gridded Nomenclature For Reporting (GNFR) source categories. The assigned isotopic signatures are shown in Table 2 and were obtained from Brass and Röckmann (2010) and Menoud et al. (2022). Source-specific emission fractions

https://doi.org/10.5194/egusphere-2026-1813
Preprint. Discussion started: 11 May 2026

GNFR category	Name	Description	^{13}C [‰]	^{2}H [‰]
A	Energy	Public electricity and heat production	-42	-175
B	Industrial	Industry (incl. oil and gas production and refining)	-60	-175
C	Residential	Other stationary combustion (residential)	-32	-175
D + E	Natural gas	Fugitives (incl. distribution of natural gas) + Solvent use	-42	-175
F + G + H + I	Transport	Road transport + Shipping + Aviation + Other mobile sources	-20	-175
J	Waste	Waste treatment (solid and liquid)	-54	-293
K + L	Agriculture	Agriculture (livestock and other)	-64	-319
None	River	The Elbe River	-66	-302
None	Background	Background	-47	-86

Table 2. Gridded Nomenclature For Reporting (GNFR) source categories and corresponding ^{13}C and ^{2}H source signatures. Isotopic values for the GNFR categories were obtained from Menoud et al. (2022), the background was the average of the background values from the continuous measurements, and the river values are the averages of local river samples.

were multiplied with isotopic signatures of the various categories from Table 2 and summed up to derive total ^{13}C and ^{2}H isotopic signatures of the CH_4 that was picked up by the air parcel along the trajectory.

3 Results and Discussion

3.1 Time series

175 The continuous time series of measured and simulated CH_4 mole fraction, ^{2}H and ^{13}C are shown in Figure 2. Generally, the CH_4 mole fraction increased during the night with an inverse effect on the ^{2}H and ^{13}C values, resulting in a clear diurnal cycle. Nighttime enhancements are common for tracers emitted at the surface, since the emissions accumulate in a shallower and more stable boundary layer during night compared to daytime. In addition to these regular enhancements, unexpected short sharp peaks were observed, with a maximum mole fraction up to 4500 ppb on 8 September 2022.

18 The simulations reproduce the general trends of the observations for CH_4, ^{2}H and ^{13}C, but do not show any sharp peaks. In contrast to the observations, the simulations exhibit the highest CH_4 enhancements during the winter season. The sharp peaks are not simulated as they likely originated from local sources that are either absent in the emission inventory or strongly smoothed out both in space and time in the inventory. The simulated enhancements generally have a reduced amplitude in comparison with the measurements. This is a known general phenomenon when comparing measurements at point locations to

185 simulated mole fractions that distribute emissions within larger grid cells. Although a Lagrangian Transport Model was used, for which resolution is not a problem of the transport itself, the effect is considerably large in our study. This arises because in an urban location, strong sources can be located close to the sampling point, and the relatively coarse resolution of the utilised emission inventory reduces the model's sensitivity to these local sources. Furthermore, the resolution of the input meteorology for the transport model was rather coarse and consequently, the simulated footprints lack fine structure on the local scale. In

https://doi.org/10.5194/egusphere-2026-1813
Preprint. Discussion started: 11 May 2026

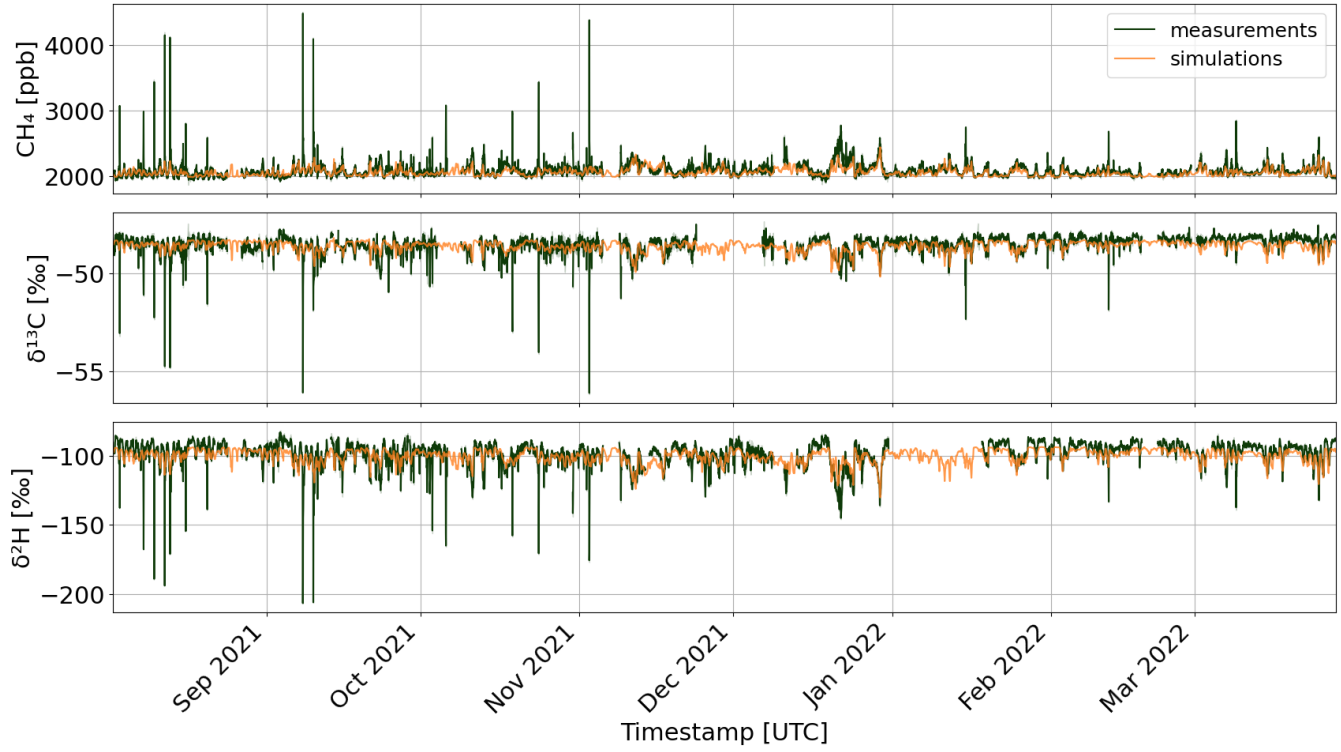

Figure 2. Time series of CH_4 mole fraction [ppb], ^{13}C VPDB [‰] and ^{2}H VSMOW [‰] taken from from the IRMS measurements (black) and model simulation (orange).

addition, it is well known that atmospheric models tend to underestimate stability and tracer accumulation in stable nighttime boundary layers, which were responsible for many of the observed peak events.

The transport model quantifies the individual contributions from each source category to the total emissions. Fig. A1 in the appendix shows that 75% of the CH_4 emissions originate from natural or biogenic sources, predominantly agriculture (52%) and waste (23%). Thermogenic emissions originate mainly from natural gas (14%).

3.2 Sources

Using the Keeling plot approach explained in section 2, we determined the isotopic source signatures of individual peaks. Figure 3 presents a dual isotope plot of these source signatures, including the sharp peaks in the measurements as well as diurnal peaks from both measurements and simulations. Most source signatures in the dual isotope plot overlay the area that is characteristic for microbial fermentation, suggesting that this is the dominant source category across all datasets. However, the diurnal peaks from both the measurements and the simulations also indicate occasional contributions from more isotopically enriched sources, whereas the sharp peaks are isotopically exclusively microbial.

https://doi.org/10.5194/egusphere-2026-1813
Preprint. Discussion started: 11 May 2026

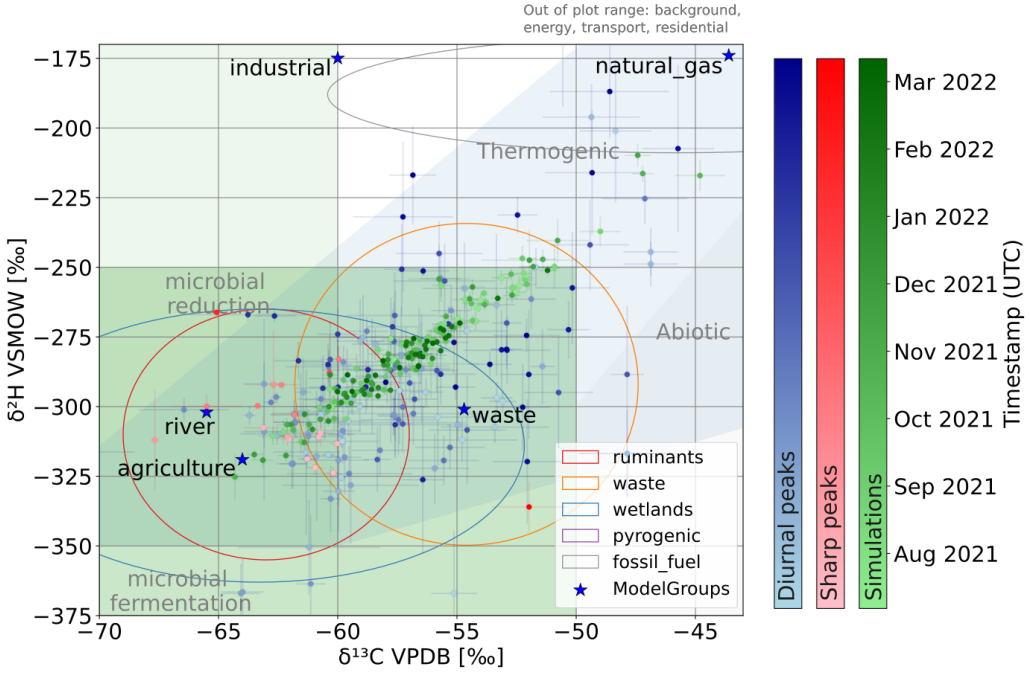

Figure 3. Dual isotope plot of all the enhancements found in the simulated timeseries and for the measurements, both the sharp peaks and the diurnal peaks. The three categories all have a different colour scale.

The source signatures derived from the diurnal measurements cover a wide range between -45‰ and -75‰ for ^{13}C, and between -175‰ and -375‰ for ^{2}H. The heavier source signatures occur more often in winter compared to summer. This pattern may reflect an increased relative contribution from thermogenic or pyrogenic sources during winter, such as enhanced oil and gas usage. The measured CH_4 mole fraction is higher in summer than in winter, likely caused by a reduction in emissions from microbial sources at cold winter temperatures.

The sharp peaks exhibit a well-defined average isotopic composition of ^{13}C = -61.9 ± 3.2‰ and ^{2}H = -307 ± 15‰. This isotopic range is considerably narrower than that observed for both the diurnal peaks and the simulations. The limited variability and characteristic isotopic signature suggest that these emissions originate from a well-defined microbial fermentation source. The sharp peaks occur more frequently in autumn than in winter, likely reflecting enhanced microbial activity at higher temperatures. In addition, these peaks are predominantly associated with southern wind. Such wind conditions transport air masses from the Elbe River, the harbour area, and nearby wastewater treatment facilities, indicating potential emissions from microbial CH_4 sources located in or near the river. One sharp peak exhibits an anomalous source signature with ^{13}C = -52‰ and ^{2}H = -337‰, falling outside the typical isotopic range of the other sharp peaks. This event occurred on 5 March with northwestern wind and represents the only sharp peak observed during winter. The footprint preceding this event (Fig.C4) indicates that the wind was very variable, thereby making it impossible to identify a distinct source.

https://doi.org/10.5194/egusphere-2026-1813
Preprint. Discussion started: 11 May 2026

The source signatures derived from the simulated time series display a linear and very tight relationship between ^{2}H and ^{13}C. This tight correlation suggests a mixing between two source components, one depleted and one enriched in both heavy isotopes. According to the simulations, three source categories account for approximately 90% of the total CH_4 enhancements:
22 natural gas (^{13}C = -43.6‰, ^{2}H = -174‰), agriculture (^{13}C = -64‰, ^{2}H = -319‰), and waste (^{13}C = -54.7‰, ^{2}H = -301‰). As the emissions of waste are relatively stable, the isotopic source signature is mainly dependent on the other two end members. Therefore, any mixture between these dominant sources produces a strongly correlated linear relationship between ^{13}C and ^{2}H.

3.2.1 Fossil emissions

225 Only nine CH_4 enhancements with a large contribution from fossil sources (^{2}H > -250 ‰, ^{13}C > -50‰) were detected during the measurement period, with no apparent seasonal dependence. Three originated from the northwest and one from the east. Although highways and industrial areas are present in these directions, no dominant fossil source was identified. Maazallahi et al. (2020) reported widespread occurrences of leakages from the natural gas distribution network in the residential areas of Hamburg. Such leakages occur randomly and can be large, but are not represented in emission inventories (Maazallahi et al.,
23 2023).

As shown in Fig. 3, the simulations are dominated by a mixture of agricultural and natural gas sources. At the same time, the number of simulated CH_4 peaks with a strong contribution from fossil sources is small and microbial emissions contribute the most. The fossil contribution in the simulations is lower than the measured ones, indicating that the model may underestimate the fossil contribution, consistent with the suggestion that they may originate from undocumented emissions, e.g. from the gas
235 distribution network.

3.3 Correlation with environmental parameters

3.3.1 Air mass origin

The wind rose for the entire IRMS measurement period (01-08-2021 to 29-03-2022) reveals a dominant wind direction from the west (Fig. 4a). Using the Yamartino method (Yamartino, 1984), the mean wind direction for the entire dataset was 219.1
24 ± 1.4 , with an average wind speed of 3.2 ± 1.9 m/s. The wind rose for the diurnal peaks is similar to the overall wind rose, confirming that CH_4 peaks are observed during all wind directions.

Figure 4c presents the wind direction measured during the periods associated with the occurrence of the sharp peaks. These peaks originate almost exclusively from the southeast (130° and 200°) and are associated with low wind speeds (between 1 and 6 m/s). This direction corresponds to the Elbe River and the harbour area. This was confirmed by footprint analysis, shown in
245 the appendix (Fig. C2).

For the diurnal peaks, we observed that the isotopic source signature varied with wind direction. The dual isotope plot, coloured by wind direction (appendix, Fig. B1), indicates that isotopically enriched thermogenic contributions primarily originated from the east (50°–135°) and northwest (260°–360°), whereas western winds were primarily associated with microbial

https://doi.org/10.5194/egusphere-2026-1813
Preprint. Discussion started: 11 May 2026

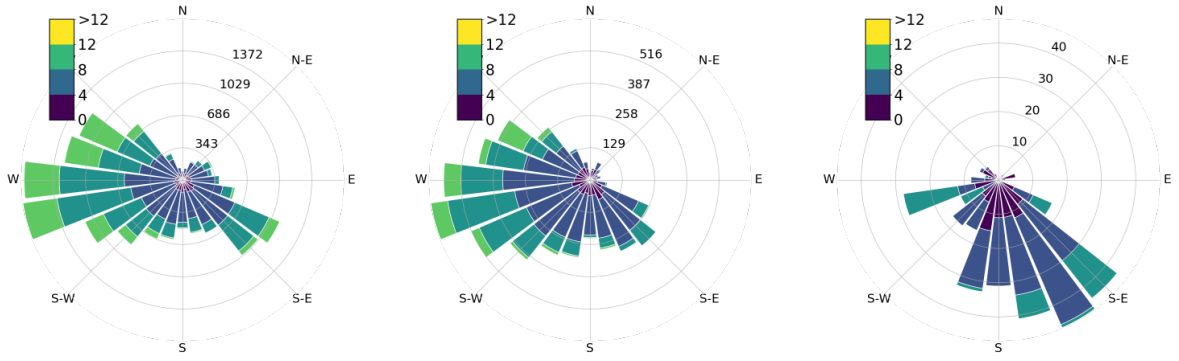

(a) (b) (c)

Figure 4. Comparison of wind conditions at the continuous measurement location coloured by the wind speed (m/s). The plots are (a) full campaign period, (b) the diurnal peaks and (c) periods when sharp CH_4 peaks were observed.

sources. This pattern is related to the higher intensity of agricultural activities toward the northwest relative to the east. Only a small number of diurnal peaks were detected from the northwest, suggesting a relative scarcity of local emission sources in this sector.

3.3.2 Boundary layer height

The boundary layer height (BLH) influences the measured CH_4 mole fractions. In general, elevated CH_4 levels were observed with a low BLH, reflecting reduced vertical mixing and the accumulation of surface emissions with a shallow boundary layer. Most diurnal CH_4 enhancements occurred when the BLH was low, although some peaks appeared independent of the BLH. The sharp peaks were consistently detected when the BLH was below 600 m, as confirmed by both the ERA5 and LIDAR datasets shown in the appendix (Fig. D1).

3.3.3 Elbe water level

Fig. 5 shows the offsets of the peaks relative to low tide. This shows that the sharp peaks predominantly occur during or just before low tide, while this relationship is much weaker for the diurnal peaks. The sharp peaks occurred more often with wind speeds between 2 and 6 m/s, a BLH below 600 m and a wind direction between 130° and 200°. A few sharp peaks are observed further from the low tide. These either occurred during periods of higher boundary layer height, originated from a non-Elbe wind direction and/or occurred with faster winds. Therefore, these sharp peaks are likely related to a different source.

A subset of the CH_4 mole fraction timeseries, overlaid with the Elbe water level, is shown in the appendix (Fig. D1). It shows sharp peaks shortly after low tide during the example period. The peaks are coloured by wind direction, confirming a southeastern wind.

https://doi.org/10.5194/egusphere-2026-1813
Preprint. Discussion started: 11 May 2026

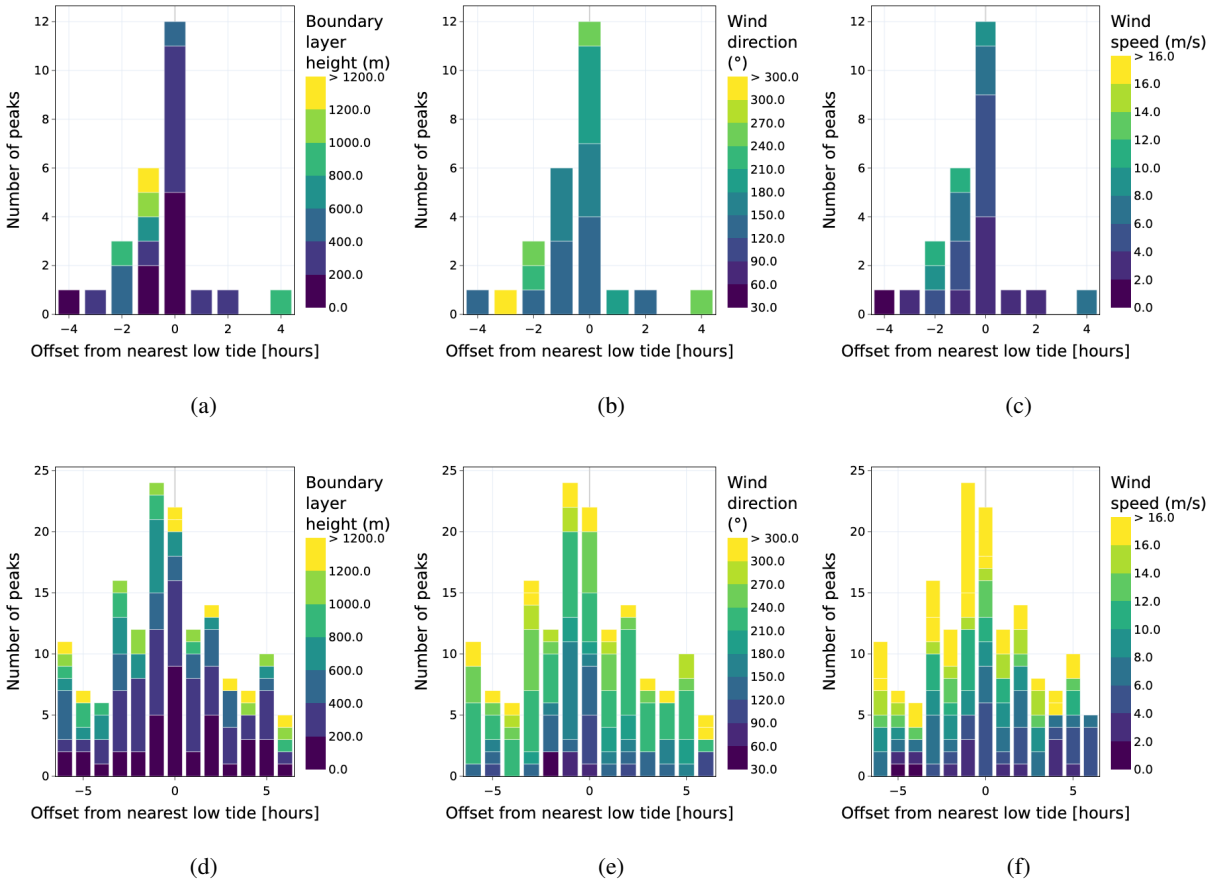

Figure 5. Panels showing the timing of the peak top relative to low tide. The top row corresponds to the sharp peaks, whereas the bottom row corresponds to the diurnal peaks. The colour scale indicates in the first column the boundary-layer height, in the second column the wind direction, and in the third column the wind speed.

3.4 Missing sources within the simulations

The TNO GHGco inventory does not include emissions from the Elbe River. We considered the river layer important as Matoušů et al. (2018) identified substantial CH_4 emissions from the upper Elbe estuary within Hamburg and Forstmaier
27 et al. (2023) demonstrated that incorporating Elbe emissions significantly improves the accuracy of inverse modelling results. Forstmaier et al. (2023) also suggested that the original layer of CH_4 emission from the water Matoušů et al. (2018) likely underestimates the CH_4 emissions from the river. When a separate river layer was added from Matoušů et al. (2018), the simulated time series still does not reproduce the observed sharp peaks. Although the simulations showed an increased contribution from the river layer during the periods when sharp peaks were measured, this increase was much smaller than
275 the magnitude of the measured peaks. This suggests that the emission factors assigned to the river layer are likely too low.

https://doi.org/10.5194/egusphere-2026-1813
Preprint. Discussion started: 11 May 2026

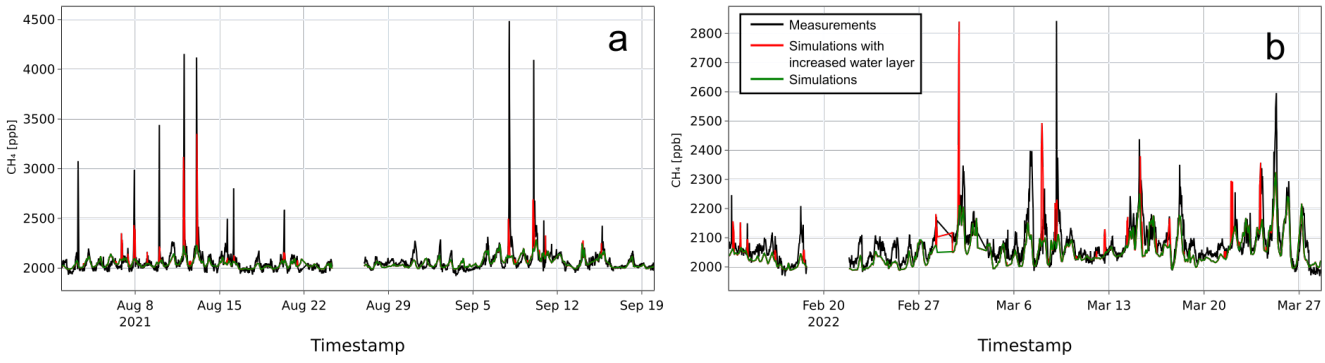

Figure 6. Exemplary CH_4 time series in August-September 2021 (a) and February-March 2022 (b). Measurements are shown in red, simulations in green and simulations with adjusted emissions from the river layer in red. The river layer emissions were adjusted by multiplying the original river layer contribution by a factor of 100 when the water level was below 600 cm, and the wind originated between 130° and 200°. This adjustment increased the total emission from the river layer by a factor of 3.8.

Importantly, the emission factor assigned to the original river layer is constant for the whole period and not related to the tide, which we concluded to be an important parameter for the sharp peaks.

When the river layer emission factor was increased by a factor of 100 under low-tide and southern wind direction conditions, most of the observed sharp peaks were successfully reproduced at magnitudes comparable to the observed ones. Two exemplary
28 sections of the timeseries with sharp peaks showing both the original and the adjusted simulations are shown in Fig. 6. Although the adjustment factor is large, it is only applied during certain conditions, making the overall increase in emissions from the river layer only a factor of 3.8. This is lower than the multiplier of 10 increase proposed by Forstmaier et al. (2023) but consistent with the range suggested by Maazallahi et al. (2020). The adjusted simulations failed to replicate the sharp peak observed on 5 March. Both the simulations and measurements indicate that this peak originates from the northwest, suggesting
285 it is unrelated to river emissions, as discussed in Section 3.2.

3.5 Measurements targeting tidal emissions

3.5.1 Stationary measurements at the Geomatikum

Unfortunately, in contrast to the initial campaign in 2022, the two weeks of CH_4 mole fraction measurements from 23-04-2024 till 02-05-2024 at the Geomatikum building did not reveal any sharp peaks. Smaller peaks occurred occasionally after low tide
29 of the Elbe River, but only exhibited a maximum CH_4 mole fraction of 2200 ppb. Fig. D2 in the appendix shows wind speed and direction during this later campaign. In this period, the wind originated mostly from the northeast or the southwest. On occasion, the wind originated from the southeast, but these conditions did not occur during low tide.

https://doi.org/10.5194/egusphere-2026-1813
Preprint. Discussion started: 11 May 2026

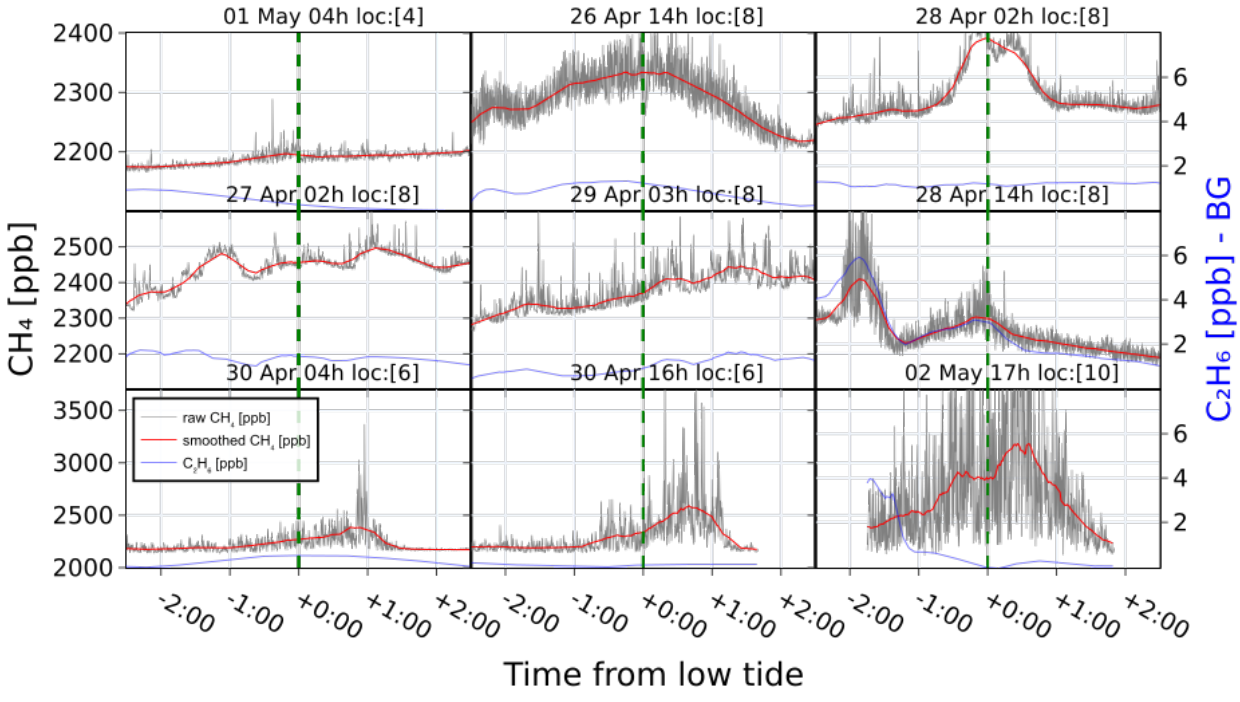

Figure 7. CH_4 time series during the stationary measurements targeting CH_4 emission from the river low tides. The time series are centred on the x-axis around the low tide time. The raw data (black) was smoothed with a 30-point running window (red). The blue line shows the 30-point smoothed C_2H_6 mole fraction with the background subtracted.

3.5.2 Stationary measurements at locations near the river

The CH_4 time series obtained with the mobile analyser during the tidal measurement campaigns at different locations are shown in Fig. 7. We regularly, but not always, observed CH_4 enhancements during or shortly after low tide. The enhancements vary strongly per location, which is not surprising since the topography, surface characteristics and the tidal movement are different per location. The first order physical process relating tides and the CH_4 emissions is the regular cycle of exposure/flooding of the river banks. Around low tide, when sediments were exposed to air, and the wind came from the direction of these sediments, we observed higher CH_4 mole fractions, indicating emissions from the exposed sediment. When the sediments re-submerged, the CH_4 mole fraction dropped quickly to the background level. Most of the CH_4 peaks encountered during the stationary measurements were not associated with concurrent C_2H_6 enhancements, clearly pointing towards biogenic rather than fossil sources. We observed a few particularly clear cases that point to tide-induced strong CH_4 emissions, which are discussed below.

https://doi.org/10.5194/egusphere-2026-1813
Preprint. Discussion started: 11 May 2026

- On 30 April, we measured at location 6, Trostbrücke and observed that the CH_4 mole fraction rose before the low tide and returned quickly to the baseline when the sediments were submerged with water again. The CH_4 increase was not associated with C_2H_6. When measuring a second time at this location, we observed a similar trend.

- From 26 April to 29 April, stationary measurements were carried out for 72 hours at the water quality station in Blankenese, located adjacent to a large wetland west of Hamburg (Measurement Location 8) (Fig. 7). In most cases, a tidal influence of CH_4 was observed, with a rise in CH_4 emissions with low tide. Other, shorter peaks in these time series might be related to fossil emissions of ships passing by, or disturbances in the water, but no clear causes could be identified.

- On 1 May, when measuring at measurement location 9 (Bunteshaus – Water Quality Station), the CH_4 mole fraction rose strongly when sediments became visible and returned to the baseline when the sediments were submerged with water. As the change in the water level was gradual, the emissions rose and the submergence process occurred over an extended period. The area of exposed sediment was large, causing CH_4 mole fractions to rise above 10 ppm. Also, gas ebullition from the sediments was observed during the water backflow phase. Similar gas ebullition leading to similarly high CH_4 mole fractions of up to 6 ppm with a notable absence of C_2H_6 was repeatedly observed at measurement location 10 (Ernst-August-Schleuse) with maximum peaks during water outflow and inflow and a sharp return to background values as soon as the sediments were covered with water. The water at this location was bubbling vividly.

At some sites where we measured during the campaign, the nearby sediments were not exposed at the lowest tides, and consequently, no clear increase in the CH_4 mole fraction was observed.

3.5.3 Source signatures of the samples

Samples collected during the mobile campaigns were analysed for isotopic composition and grouped per location. The source signatures derived from Keeling plot analyses (Appendix, Fig D3) clearly reveal a biogenic origin of the CH_4, with average source signatures of -325‰ for ^{2}H and -71‰ for ^{13}C. This supports our interpretation that these measured elevations were indeed from the river and are not strongly affected by contamination from another source type. Sample A at location 7 has an isotopic composition that reflects thermogenic contributions. This sampling location was in the city centre and the CH_4 mole fraction enhancement reached only 2070 ppb at maximum. Maazallahi et al. (2020) showed that natural gas leaks are another important source of CH_4 emissions in the city centre. Thus, these samples might be contaminated by natural gas emissions.

4 Conclusions

Strong diurnal variations with nighttime CH_4 enhancements are the main mode of variability of CH_4 observed in Hamburg, Germany in both the measurements and the simulations. Most of the measured diurnal enhancements originated from microbial sources, however, there are also regular enhancements with a thermogenic contribution. The simulations consistently underes-

https://doi.org/10.5194/egusphere-2026-1813
Preprint. Discussion started: 11 May 2026

timated the peak mole fractions, likely due to the coarse resolution of both the emission inventory and the transport model, as well as an underestimation of river emissions in the inventory.

In addition to these typical diurnal variations, irregular sharp peaks were identified in the CH_4 isotopic measurements. These peaks were associated with emissions from the Elbe River, as they only occurred when the river's water level was below 600 cm. They were further linked to specific meteorological conditions: wind directions ranging between 130° and 200° (Elbe sector), boundary layer heights (BLH) below 600 m, and wind speeds between 2 and 6 m/s. None of these sharp peaks were reproduced in the simulations, as they are linked to very localised water level variations. When the Elbe River emission factor was increased under the 'sharp peak' conditions, the model successfully reproduced the observed peaks.

The stationary measurements near the river confirmed the presence of Elbe-related CH_4 emissions. These varied across locations, but typically a CH_4 peak was observed when the river sediment was exposed and diminished again upon submergence. Isotopic analysis indicated a microbial origin of these emissions, with no concurrent C_2H_6 enhancements, supporting that the CH_4 source is biogenic, like the river. Thus, multiple lines of evidence point towards strongly enhanced low-tide emissions of a CH_4 as the source of the sharp peaks observed in the long-time stationary measurement campaign.

Rivers are not yet commonly included as a separate layer in CH_4 emission inventories. We show here that rivers strongly contribute to observed CH_4 variability with a distinct isotopic signature. In cases where river emissions are included in the CH_4 emission inventories or when separate layers are used for climate models, they are often represented as constant values in the climate model. Our results show that for rivers influenced by tidal cycles, such as the Elbe River, emissions increased substantially during low tide, a pattern likely to apply to other rivers. Recognising the temporal and spatial variability of river emissions may lead to novel, effective mitigation measures, such as river dredging below the lowest tide. More advanced inclusion of river emissions in emission inventories will increase the accuracy of atmospheric transport models, improving greenhouse gas modelling and providing more complete input for the development and evaluation of mitigation strategies. Additionally, the comparison between our measurements and simulations demonstrates that a finer spatial resolution is necessary to capture the large spatial variability of emissions in cities. Furthermore, the observed isotopic variability is much higher than the modelled one. This could be addressed by increasing the number of source categories and incorporating more local point source measurements when interpreting city observations.

Data availability. The data is available on the ICOS carbon portal under DOI 10.18160/NXYQ-Y64M

Author contributions. **Jacoline van Es**: Writing, data analysis, figure and table creation, in-situ measurements, bag sample analysis; **Juan Bettinelli**: data-analysis, in situ-analysis; **Jia Chen**: design of experiment, discussions throughout the process, funding; **Carina van der Veen**: System installation, bag sample analysis; **Stephan Henne**: Langranian transport model, trajectory plots; **Thomas Röckmann**: design of experiment, data analysis, writing, funding.

https://doi.org/10.5194/egusphere-2026-1813
Preprint. Discussion started: 11 May 2026

Competing interests. None of the authors had a competing interest.

A*cknowledgements.* This study received financial support from the Environmental Defense Fund, the H2020 Marie Skłodowska-Curie Actions through the project "Methane goes Mobile – Measurements and Modelling", grant no. 722479, the European Union's Horizon Europe Research and Innovation Programme under, HORIZON-CL5-2022-D1-02 Grant Agreement No 101081430, project PARIS and the Ruisdael Observatory, a scientific research infrastructure project which is (partly) financed by the Dutch Research Council (NWO; grant no. 184.034.015) and the European Union's Horizon 2020 programme (Grant 101037319) in the framework of the ICOS Cities project and by the European Research Council (ERC) Consolidator Grant CoSense4Climate (Grant 101089203).

https://doi.org/10.5194/egusphere-2026-1813
Preprint. Discussion started: 11 May 2026

References

Brass, M. and Röckmann, T.: Continuous-Flow Isotope Ratio Mass Spectrometry Method for Carbon and Hydrogen Isotope Measurements on Atmospheric Methane, Atmospheric Measurement Techniques, 3, 1707–1721, https://doi.org/10.5194/amt-3-1707-2010, 2010.

Calvin, K., Dasgupta, D., Krinner, G., Mukherji, A., Thorne, P. W., Trisos, C., Romero, J., Aldunce, P., Barrett, K., Blanco, G., Cheung, W. W., Connors, S., Denton, F., Diongue-Niang, A., Dodman, D., Garschagen, M., Geden, O., Hayward, B., Jones, C., Jotzo, F., Krug, T., Lasco, R., Lee, Y.-Y., Masson-Delmotte, V., Meinshausen, M., Mintenbeck, K., Mokssit, A., Otto, F. E., Pathak, M., Pirani, A., Poloczanska, E., Pörtner, H.-O., Revi, A., Roberts, D. C., Roy, J., Ruane, A. C., Skea, J., Shukla, P. R., Slade, R., Slangen, A., Sokona, Y., Sörensson, A. A., Tignor, M., Van Vuuren, D., Wei, Y.-M., Winkler, H., Zhai, P., Zommers, Z., Hourcade, J.-C., Johnson, F. X., Pachauri, S., Simpson, N. P., Singh, C., Thomas, A., Totin, E., Arias, P., Bustamante, M., Elgizouli, I., Flato, G., Howden, M., Méndez-Vallejo, C., Pereira, J. J., Pichs-Madruga, R., Rose, S. K., Saheb, Y., Sánchez Rodríguez, R., Ürge-Vorsatz, D., Xiao, C., Yassaa, N., Alegría, A., Armour, K., Bednar-Friedl, B., Blok, K., Cissé, G., Dentener, F., Eriksen, S., Fischer, E., Garner, G., Guivarch, C., Haasnoot, M., Hansen, G., Hauser, M., Hawkins, E., Hermans, T., Kopp, R., Leprince-Ringuet, N., Lewis, J., Ley, D., Ludden, C., Niamir, L., Nicholls, Z., Some, S., Szopa, S., Trewin, B., Van Der Wijst, K.-I., Winter, G., Witting, M., Birt, A., Ha, M., Romero, J., Kim, J., Haites, E. F., Jung, Y., Stavins, R., Birt, A., Ha, M., Orendain, D. J. A., Ignon, L., Park, S., Park, Y., Reisinger, A., Cammaramo, D., Fischlin, A., Fuglestvedt, J. S., Hansen, G., Ludden, C., Masson-Delmotte, V., Matthews, J. R., Mintenbeck, K., Pirani, A., Poloczanska, E., Leprince-Ringuet, N., and Péan, C.: IPCC, 2023: Climate Change 2023: Synthesis Report. Contribution of Working Groups I, II and III to the Sixth Assessment Report of the Intergovernmental Panel on Climate Change [Core Writing Team, H. Lee and J. Romero (Eds.)]. IPCC, Geneva, Switzerland., Tech. rep., Intergovernmental Panel on Climate Change (IPCC), https://doi.org/10.59327/IPCC/AR6-9789291691647, 2023.

Dietrich, F., Chen, J., Shekhar, A., Lober, S., Krämer, K., Leggett, G., van der Veen, C., Velzeboer, I., Denier van der Gon, H., and Röckmann, T.: Climate Impact Comparison of Electric and Gas-Powered End-User Appliances, Earth's Future, 11, e2022EF002 877, https://doi.org/10.1029/2022EF002877, 2023.

Eyer, S., Tuzson, B., Popa, M. E., van der Veen, C., Röckmann, T., Rothe, M., Brand, W. A., Fisher, R., Lowry, D., Nisbet, E. G., Brennwald, M. S., Harris, E., Zellweger, C., Emmenegger, L., Fischer, H., and Mohn, J.: Real-Time Analysis of ^{13}C- and D-CH_4 in Ambient Air with Laser Spectroscopy: Method Development and First Intercomparison Results, Atmospheric Measurement Techniques, 9, 263–280, https://doi.org/10.5194/amt-9-263-2016, 2016.

Forstmaier, A., Chen, J., Dietrich, F., Bettinelli, J., Maazallahi, H., Schneider, C., Winkler, D., Zhao, X., Jones, T., van der Veen, C., Wildmann, N., Makowski, M., Uzun, A., Klappenbach, F., Denier van der Gon, H., Schwietzke, S., and Röckmann, T.: Quantification of Methane Emissions in Hamburg Using a Network of FTIR Spectrometers and an Inverse Modeling Approach, Atmospheric Chemistry and Physics, 23, 6897–6922, https://doi.org/10.5194/acp-23-6897-2023, 2023.

Hersbach, H., Bell, B., Berrisford, P., Hirahara, S., Horányi, A., Muñoz-Sabater, J., Nicolas, J., Peubey, C., Radu, R., Schepers, D., Simmons, A., Soci, C., Abdalla, S., Abellan, X., Balsamo, G., Bechtold, P., Biavati, G., Bidlot, J., Bonavita, M., De Chiara, G., Dahlgren, P., Dee, D., Diamantakis, M., Dragani, R., Flemming, J., Forbes, R., Fuentes, M., Geer, A., Haimberger, L., Healy, S., Hogan, R. J., Hólm, E., Janisková, M., Keeley, S., Laloyaux, P., Lopez, P., Lupu, C., Radnoti, G., de Rosnay, P., Rozum, I., Vamborg, F., Villaume, S., and Thépaut, J.-N.: The ERA5 Global Reanalysis, Quarterly Journal of the Royal Meteorological Society, 146, 1999–2049, https://doi.org/10.1002/qj.3803, 2020.

https://doi.org/10.5194/egusphere-2026-1813
Preprint. Discussion started: 11 May 2026

Hopkins, F. M., Ehleringer, J. R., Bush, S. E., Duren, R. M., Miller, C. E., Lai, C.-T., Hsu, Y.-K., Carranza, V., and Randerson, J. T.: Mitigation of Methane Emissions in Cities: How New Measurements and Partnerships Can Contribute to Emissions Reduction Strategies, Earth's Future, 4, 408–425, https://doi.org/10.1002/2016EF000381, 2016.

Keeling, C. D.: The Concentration and Isotopic Abundances of Carbon Dioxide in Rural and Marine Air, Geochimica et Cosmochimica Acta, 24, 277–298, https://doi.org/10.1016/0016-7037(61)90023-0, 1961.

Kuenen, J., Dellaert, S., Visschedijk, A., Jalkanen, J.-P., Super, I., and Denier van der Gon, H.: CAMS-REG-v4: A State-of-the-Art High-Resolution European Emission Inventory for Air Quality Modelling, Earth System Science Data, 14, 491–515, https://doi.org/10.5194/essd-14-491-2022, 2022.

Maazallahi, H., Fernandez, J. M., Menoud, M., Zavala-Araiza, D., Weller, Z. D., Schwietzke, S., Von Fischer, J. C., Denier Van Der Gon, H., and Röckmann, T.: Methane Mapping, Emission Quantification, and Attribution in Two European Cities: Utrecht (NL) and Hamburg (DE), Atmospheric Chemistry and Physics, 20, 14 717–14 740, https://doi.org/10.5194/acp-20-14717-2020, 2020.

Maazallahi, H., Delre, A., Scheutz, C., Fredenslund, A. M., Schwietzke, S., Denier van der Gon, H., and Röckmann, T.: Intercomparison of Detection and Quantification Methods for Methane Emissions from the Natural Gas Distribution Network in Hamburg, Germany, Atmospheric Measurement Techniques, 16, 5051–5073, https://doi.org/10.5194/amt-16-5051-2023, 2023.

Matoušů, A., Osudar, R., imek, K., and Bussmann, I.: Methane Distribution and Methane Oxidation in the Water Column of the Elbe Estuary, Germany, Aquatic Sciences, 79, 443–458, https://doi.org/10.1007/s00027-016-0509-9, 2017.

Matoušů, A., Rulík, M., Tušer, M., Bednařík, A., imek, K., and Bussmann, I.: Methane Dynamics in a Large River: A Case Study of the Elbe River, Aquatic Sciences, 81, 12, https://doi.org/10.1007/s00027-018-0609-9, 2018.

Menoud, M., Van Der Veen, C., Necki, J., Bartyzel, J., Szénási, B., Stanisavljević, M., Pison, I., Bousquet, P., and Röckmann, T.: Methane (CH4) Sources in Krakow, Poland: Insights from Isotope Analysis, Atmospheric Chemistry and Physics, 21, 13 167–13 185, https://doi.org/10.5194/acp-21-13167-2021, 2021.

Menoud, M., Van Der Veen, C., Lowry, D., Fernandez, J. M., Bakkaloglu, S., France, J. L., Fisher, R. E., Maazallahi, H., Stanisavljević, M., Nęcki, J., Vinkovic, K., Łakomiec, P., Rinne, J., Korbeń, P., Schmidt, M., Defratyka, S., Yver-Kwok, C., Andersen, T., Chen, H., and Röckmann, T.: New Contributions of Measurements in Europe to the Global Inventory of the Stable Isotopic Composition of Methane, Earth System Science Data, 14, 4365–4386, https://doi.org/10.5194/essd-14-4365-2022, 2022.

Openstreetmap: OpenStreetMap Data, https://www.openstreetmap.org/.

Pataki, D. E., Ehleringer, J. R., Flanagan, L. B., Yakir, D., Bowling, D. R., Still, C. J., Buchmann, N., Kaplan, J. O., and Berry, J. A.: The Application and Interpretation of Keeling Plots in Terrestrial Carbon Cycle Research, Global Biogeochemical Cycles, 17, 2001GB001 850, https://doi.org/10.1029/2001GB001850, 2003.

Port of Hamburg Marketing: Tides in the River Elbe, https://www.hafen-hamburg.de/en/portofhamburg/tide/.

Röckmann, T., Eyer, S., Van Der Veen, C., Popa, M. E., Tuzson, B., Monteil, G., Houweling, S., Harris, E., Brunner, D., Fischer, H., Zazzeri, G., Lowry, D., Nisbet, E. G., Brand, W. A., Necki, J. M., Emmenegger, L., and Mohn, J.: In Situ Observations of the Isotopic Composition of Methane at the Cabauwtall Tower Site, Atmospheric Chemistry and Physics, 16, 10 469–10 487, https://doi.org/10.5194/acp-16-10469-2016, 2016.

Röckmann, T., Menoud, M., van Es, J., van der Veen, C., Maazallahi, H., Jagoda, P., Necki, J. M., Bartyzel, J., Korben, P., Defratyka, S., Schmidt, M., Corbu, M., Iancu, S., Calcan, A., Ardelean, M., Ghemulet, S., Pop, C., Radovici, A., Mereuta, A., Stefanie, H., and Baciu, C.: Measurement Report: Isotopic Composition of CH_4 Emitted from Gas Exploration Sites in the Transylvanian Basin, Romania, EGUsphere, pp. 1–9, https://doi.org/10.5194/egusphere-2025-4461, 2025.

https://doi.org/10.5194/egusphere-2026-1813
Preprint. Discussion started: 11 May 2026

Rogelj, J. and Lamboll, R. D.: Substantial Reductions in Non-CO2 Greenhouse Gas Emissions Reductions Implied by IPCC Estimates of the Remaining Carbon Budget, Communications Earth & Environment, 5, 35, https://doi.org/10.1038/s43247-023-01168-8, 2024.

Saunois, M., Stavert, A. R., Poulter, B., Bousquet, P., Canadell, J. G., Jackson, R. B., Raymond, P. A., Dlugokencky, E. J., Houweling, S., Patra, P. K., Ciais, P., Arora, V. K., Bastviken, D., Bergamaschi, P., Blake, D. R., Brailsford, G., Bruhwiler, L., Carlson, K. M., Carrol, M., Castaldi, S., Chandra, N., Crevoisier, C., Crill, P. M., Covey, K., Curry, C. L., Etiope, G., Frankenberg, C., Gedney, N., Hegglin, M. I., Höglund-Isaksson, L., Hugelius, G., Ishizawa, M., Ito, A., Janssens-Maenhout, G., Jensen, K. M., Joos, F., Kleinen, T., Krummel, P. B., Langenfelds, R. L., Laruelle, G. G., Liu, L., Machida, T., Maksyutov, S., McDonald, K. C., McNorton, J., Miller, P. A., Melton, J. R., Morino, I., Müller, J., Murguia-Flores, F., Naik, V., Niwa, Y., Noce, S., O'Doherty, S., Parker, R. J., Peng, C., Peng, S., Peters, G. P., Prigent, C., Prinn, R., Ramonet, M., Regnier, P., Riley, W. J., Rosentreter, J. A., Segers, A., Simpson, I. J., Shi, H., Smith, S. J., Steele, L. P., Thornton, B. F., Tian, H., Tohjima, Y., Tubiello, F. N., Tsuruta, A., Viovy, N., Voulgarakis, A., Weber, T. S., van Weele, M., van der Werf, G. R., Weiss, R. F., Worthy, D., Wunch, D., Yin, Y., Yoshida, Y., Zhang, W., Zhang, Z., Zhao, Y., Zheng, B., Zhu, Q., Zhu, Q., and Zhuang, Q.: The Global Methane Budget 2000–2017, Earth System Science Data, 12, 1561–1623, https://doi.org/10.5194/essd-12-1561-2020, 2020.

Seibert, P. and Frank, A.: Source-Receptor Matrix Calculation with a Lagrangian Particle Dispersion Model in Backward Mode, Atmospheric Chemistry and Physics, 4, 51–63, https://doi.org/10.5194/acp-4-51-2004, 2004.

Stohl, A., Forster, C., Frank, A., Seibert, P., and Wotawa, G.: Technical Note: The Lagrangian Particle Dispersion Model FLEXPART Version 6.2, Atmospheric Chemistry and Physics, 5, 2461–2474, https://doi.org/10.5194/acp-5-2461-2005, 2005.

United Nations: Paris Agreement, 2016.

van Es, J., van der Veen, C., Baciu, C., Hmoudah, M., Menoud, M., Henne, S., and Röckmann, T.: Methane Sources in Cluj-Napoca, Romania: Insights From Isotopic Analysis, Journal of Geophysical Research: Atmospheres, 130, e2024JD043 015, https://doi.org/10.1029/2024JD043015, 2025.

Vasiljević, N., Lea, G., Courtney, M., Cariou, J.-P., Mann, J., and Mikkelsen, T.: Long-Range WindScanner System, Remote Sensing, 8, 896, https://doi.org/10.3390/rs8110896, 2016.

Whiticar, M. J.: The Biogeochemical Methane Cycle, in: Hydrocarbons, Oils and Lipids: Diversity, Origin, Chemistry and Fate, edited by Wilkes, H., pp. 1–78, Springer International Publishing, Cham, ISBN 978-3-319-54529-5, https://doi.org/10.1007/978-3-319-54529-5_5-1, 2020.

Wildmann, N., Päschke, E., Roiger, A., and Mallaun, C.: Towards Improved Turbulence Estimation with Doppler Wind Lidar Velocity-Azimuth Display (VAD) Scans, Atmospheric Measurement Techniques, 13, 4141–4158, https://doi.org/10.5194/amt-13-4141-2020, 2020.

Yamartino, R. J.: A Comparison of Several "Single-Pass" Estimators of the Standard Deviation of Wind Direction, Journal of Applied Meteorology and Climatology, 23, 1362–1366, https://doi.org/10.1175/1520-0450(1984)023<1362:ACOSPE>2.0.CO;2, 1984.

https://doi.org/10.5194/egusphere-2026-1813
Preprint. Discussion started: 11 May 2026

Appendix A: Simulated time series

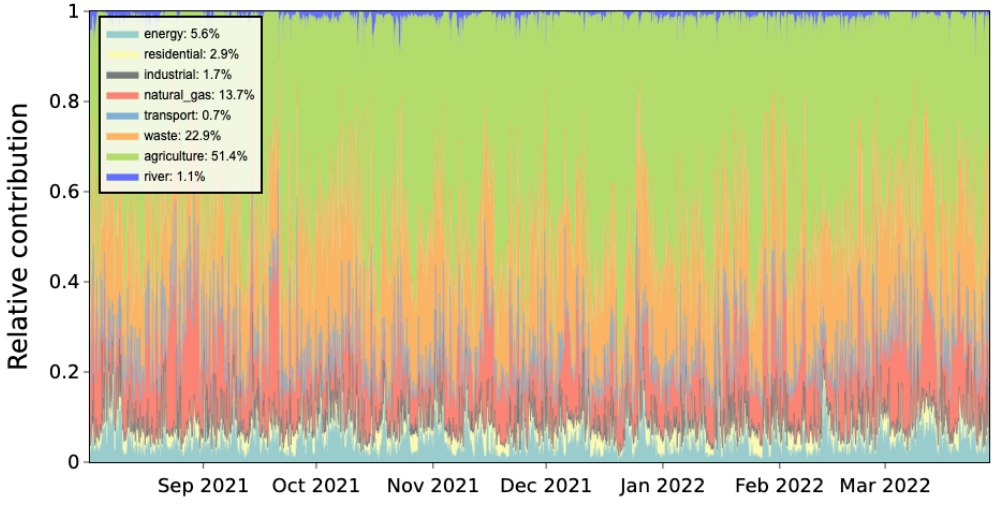

Figure A1. Time series of relative CH_4 source contributions as simulated by the FLEXPART model. The legend states the average relative contribution of each emission category for the complete timeseries.

https://doi.org/10.5194/egusphere-2026-1813
Preprint. Discussion started: 11 May 2026

Appendix B: Dual isotope plot

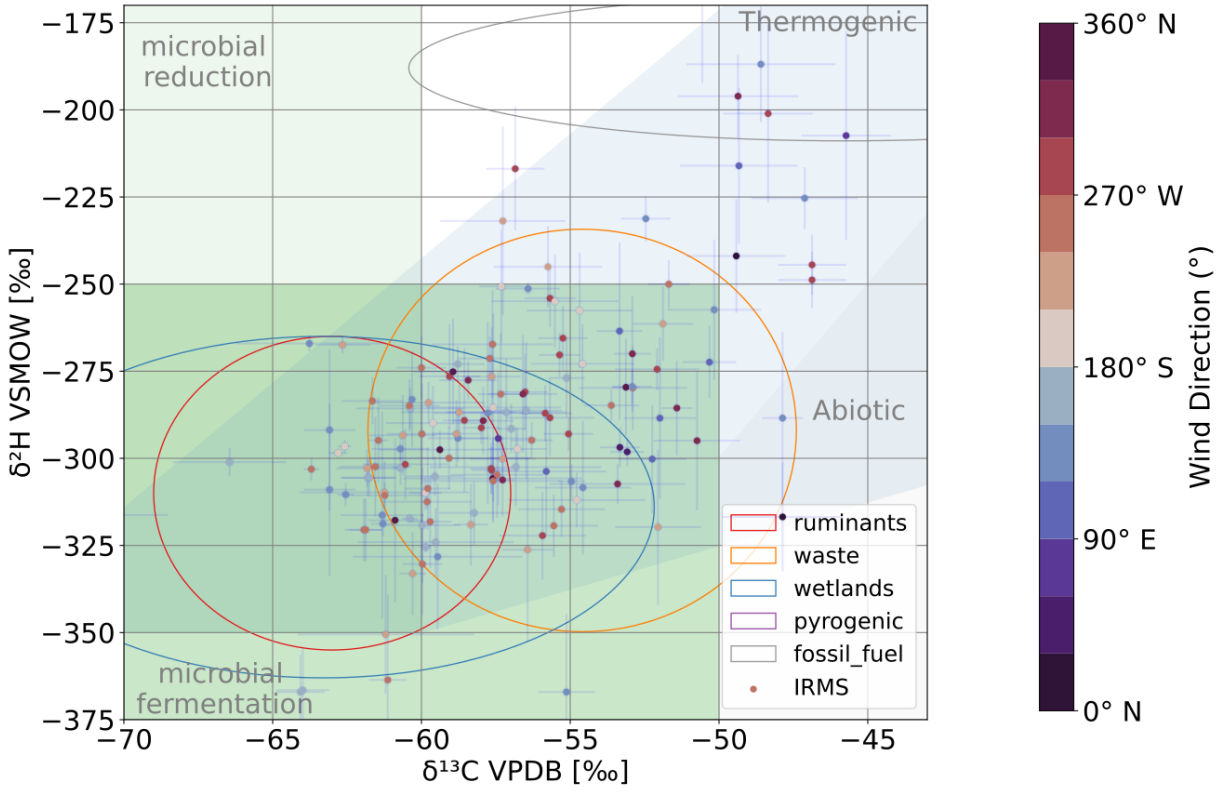

Figure B1. Dual isotope plot, coloured by the wind direction.

Appendix C: Footprints

https://doi.org/10.5194/egusphere-2026-1813
Preprint. Discussion started: 11 May 2026

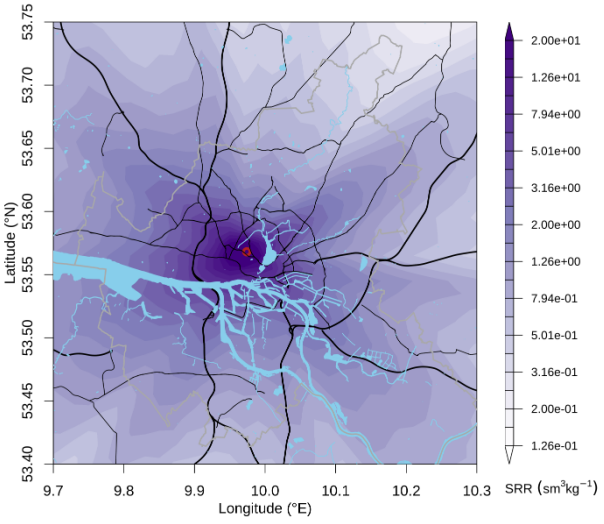

Figure C1. Average footprint during the continuous IRMS measurements

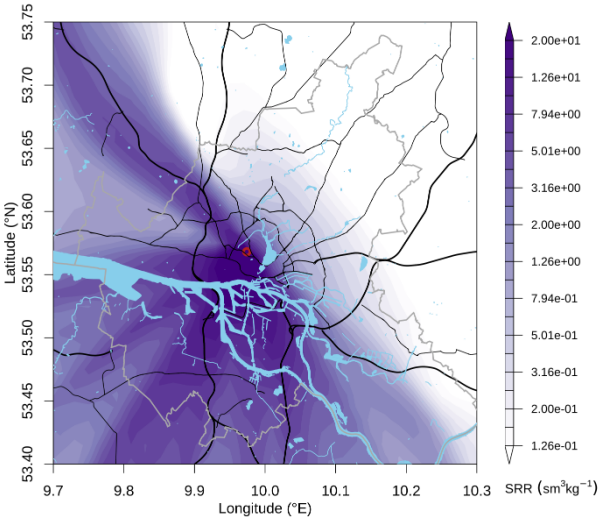

Figure C2. Average footprint of the detected sharp peaks.

https://doi.org/10.5194/egusphere-2026-1813
Preprint. Discussion started: 11 May 2026

Appendix D: Sharp peak measurements

https://doi.org/10.5194/egusphere-2026-1813
Preprint. Discussion started: 11 May 2026

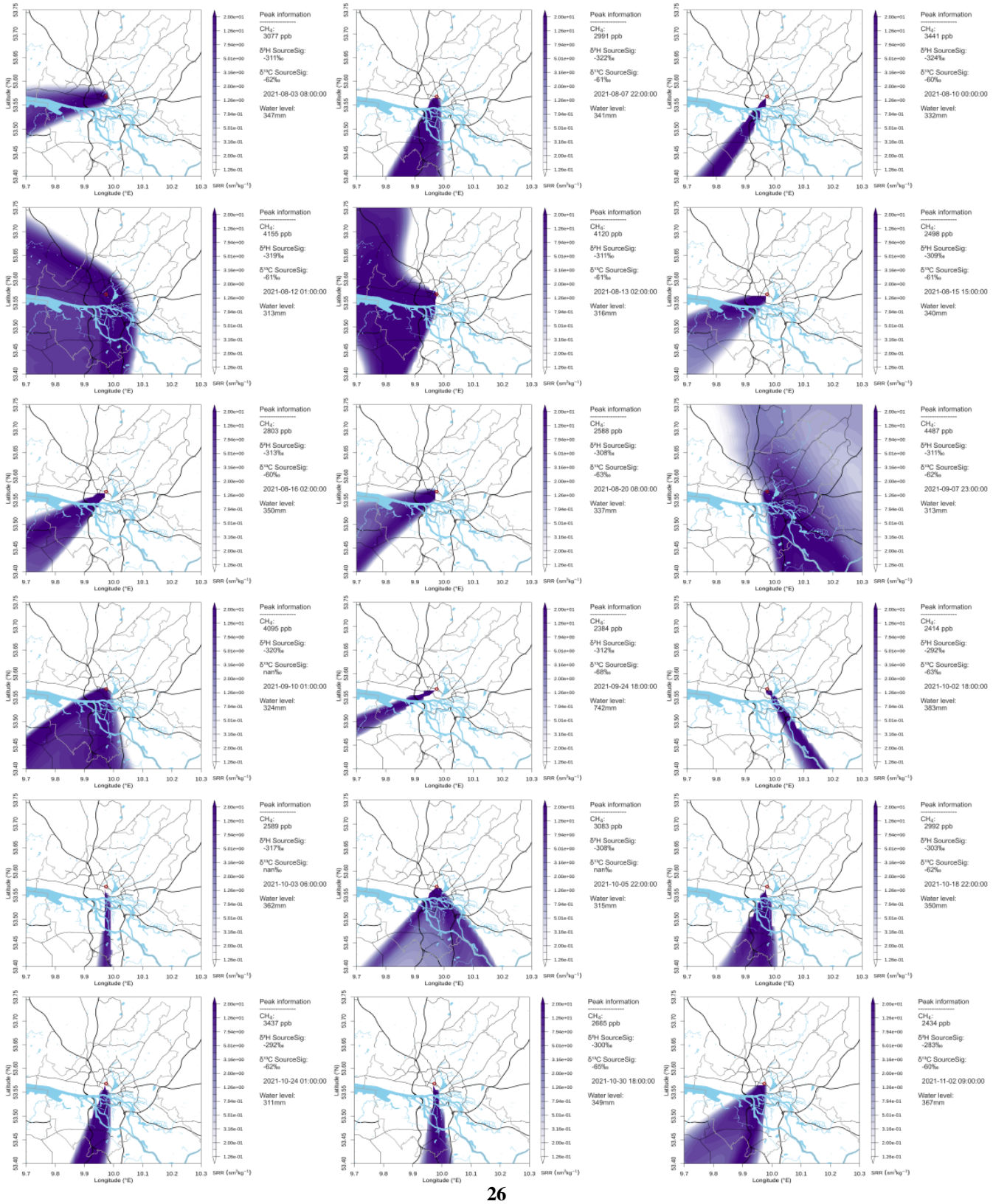

Figure C3. Footprints illustrating the spatial origin of observed sharp peaks. Each subfigure includes information on the peak time, CH_4 mole fraction, ^{13}C, ^{2}H source signatures and corresponding water level (Part 1).

https://doi.org/10.5194/egusphere-2026-1813
Preprint. Discussion started: 11 May 2026

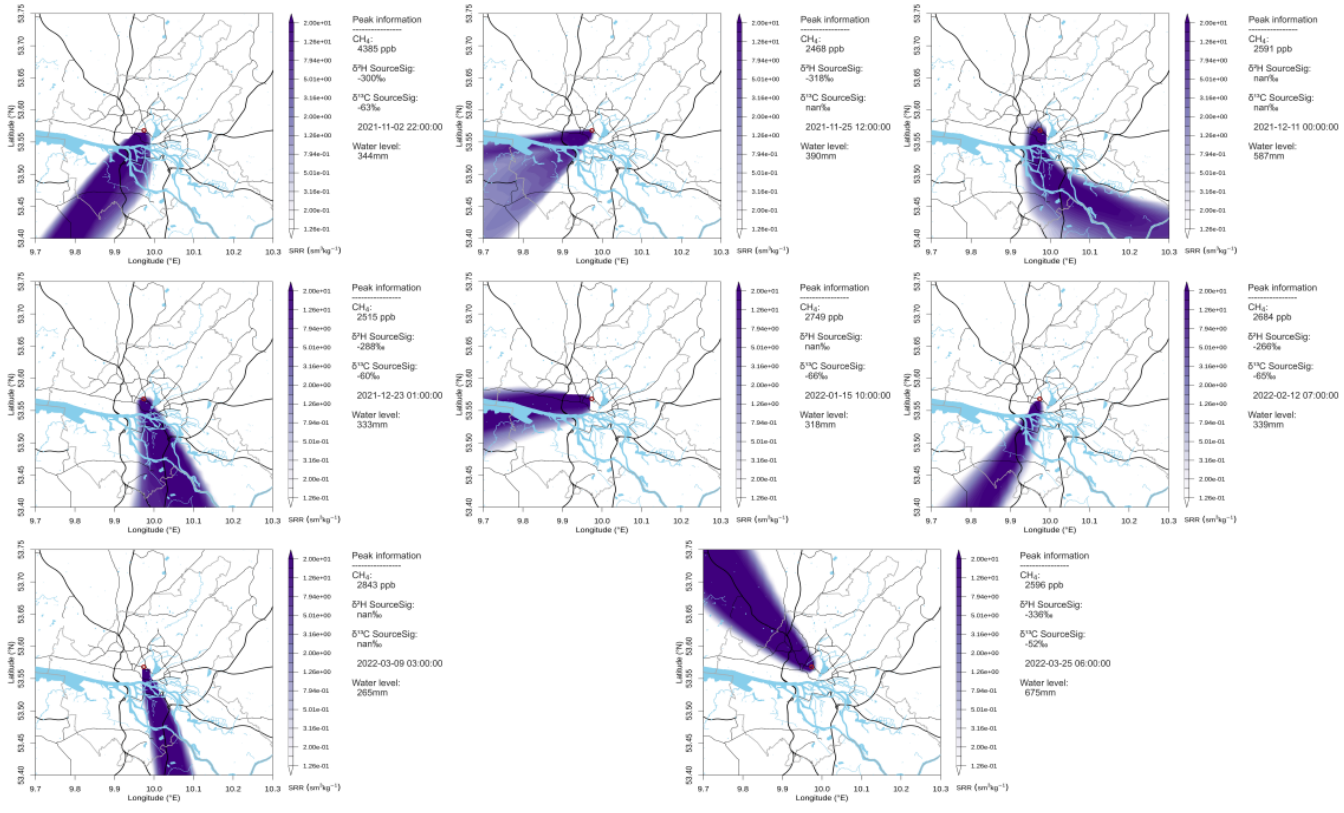

Figure C4. Footprints illustrating the spatial origin of observed sharp peaks. Each subfigure includes information on the peak time, CH_4 mole fraction, ^{13}C, ^{2}H source signatures and corresponding water level (Part 2).

https://doi.org/10.5194/egusphere-2026-1813
Preprint. Discussion started: 11 May 2026

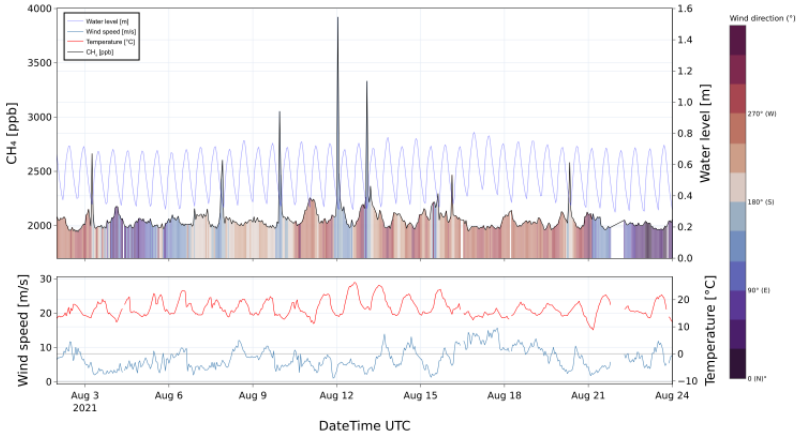

Figure D1. Subset of the continuous measurements from 01-08-2021 till 24-08-2021. The top graph shows the CH_4 mole fraction (black line), and a bar plot below the line is coloured by the wind direction. The blue line shows the water level on the right axis. The bottom panel shows the meteorological parameters wind speed and temperature.

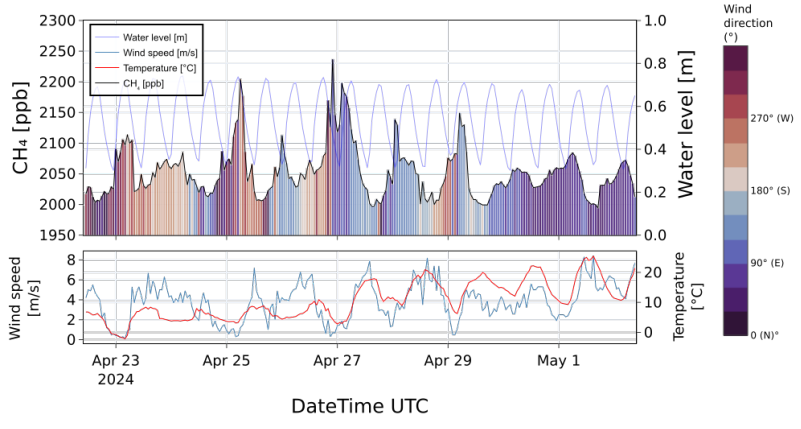

Figure D2. Timeline of CRDS CH_4 measurements (black) and Elbe water level (blue) during the 2024 measurement campaign at the Geomatikum. The CH_4 mole fraction is filled with a bar plot of the wind direction. The bottom panel shows the meteorological parameters of wind speed and temperature.

https://doi.org/10.5194/egusphere-2026-1813
Preprint. Discussion started: 11 May 2026

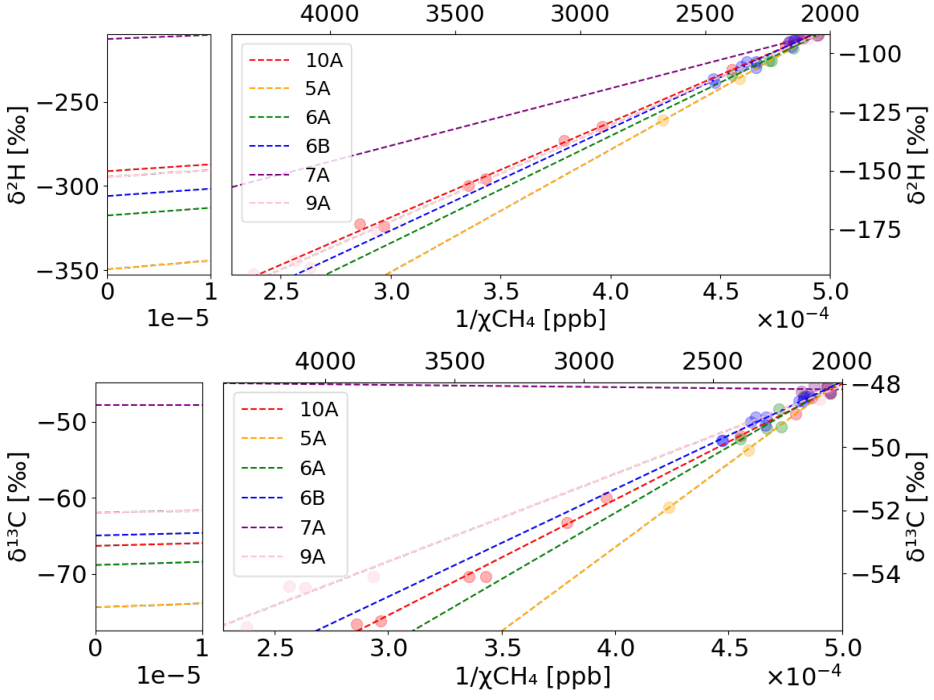

Figure D3. Keeling plots (value versus inverse of the CH_4 mole fraction) of the collected air samples. Each sampling location is represented with a unique colour. The top panel shows ^{2}H and the top panel ^{13}C.